Near-field electromagnetic trapping through curl-spin forces

Iñigo Liberal, Iñigo Ederra, Ramón Gonzalo, and Richard W. Ziolkowski

Near-Field Electromagnetic Trapping through Curl-Spin Forces

Iñigo Liberal,[1] Iñigo Ederra,[1] Ramón Gonzalo,[1] and Richard W. Ziolkowski[2]

[1]*Electrical and Electronic Engineering Department,*
Universidad Pública de Navarra, Campus Arrosadía, Pamplona, 31006 Spain
[2]*Department of Electrical and Computer Engineering, University of Arizona, Tucson, AZ, 85721 USA*

Near-field electromagnetic trapping of particles is generally obtained by means of gradient forces. In this paper, we discuss the attractive behavior of curl-spin forces, as well as their potential for near-field electromagnetic trapping and manipulation. It is demonstrated that curl-spin forces enable the trapping of particles operating at their resonant frequency. Such phenomena can be exploited to design more efficient and selective electromagnetic traps, to boost near-field energy exchange systems, and to bring stability to coupled resonant radiators. It also will be illustrated how the balance between the gradient, radiation pressure and curl-spin force components leads to the formation of zero-force rings around their sources, which explicitly demarcate the trapping regions. Analytical and numerical analyses are presented to assess the stability of the trapping mechanism.

I. INTRODUCTION

Manipulation and trapping of objects through the forces produced by electromagnetic fields has become a key methodology, for instance, in biology [1, 2], biochemistry [3], nano-fabrication [4] and atomic physics [5]. Several far-field (FF) and near-field (NF) manipulation techniques have been developed to control the location of particles. Firstly, FF techniques are based, for example, on optical tweezers [6–8] and tractor beams [9–11]. On the one hand, optical tweezers make use of focused optical beams, where the radiation pressure pushes a particle in the direction of propagation, while concurrent gradient forces keep it at the beam center. On the other hand, tractor beams exploit interference phenomena to create a dragging radiation pressure that attracts a particle towards the sources. Secondly, NF techniques are based on metal probes, tips and nano-antennas [12–15]. All of these NF techniques rely on the creation of large, highly-localized field intensities, which produce gradient forces that enable the trapping of objects in the vicinity of the source.

Notwithstanding the success of gradient force-based techniques, NF electromagnetic trapping based on absorption-scattering forces, i.e., radiation pressure and the usually disregarded curl-spin forces [16], should be investigated to open up new possibilities and to mitigate the weaknesses of the gradient force-based systems. Note that gradient forces vanish at a particle resonance [17] and, as a result, the dominant absorption-scattering force repels the particle from the source. This is highly inconvenient, especially since the particle-electromagnetic field interactions are maximized at a resonance. Moreover, since gradient forces are zero at the resonance, any benefits coming from it are lost to the trapping mechanism. This paper investigates the forces produced by a small localized source, including not only the gradient forces, but also the radiation pressure and curl-spin force components. The analysis reveals attractive forces at the resonance of a particle that originate from the curl-spin force

component. Synergies between electromagnetic trapping at a resonant frequency and other applications, such as energy transfer and emission enhancement, are also addressed.

II. ELECTROMAGNETIC FORCES PRODUCED BY A LOCALIZED SOURCE

Consider then a localized source, placed at the origin of the coordinates and modeled as a electric Hertzian dipole with current moment $I_e l$ oriented along $+\hat{\mathbf{z}}$ (see Fig. 1(a)). For the sake of simplicity, let us assume that this source and the interacting particle are embedded in free-space and that the dipole is driven with a sinusoid at the angular frequency ω. Assuming the $e^{j\omega t}$ time convention, the components of the time-harmonic electromagnetic fields produced by the Hertzian dipole: $\mathbf{E}^i = E_r^i \hat{\mathbf{r}} + E_\theta^i \hat{\boldsymbol{\theta}}$, $\mathbf{H}^i = H_\phi^i \hat{\boldsymbol{\phi}}$, are given by the closed form analytical expressions (see, e.g., Ref. 18):

$$E_r^i = \frac{\eta_0 k_0^2}{4\pi} I_e l \cdot 2\cos\theta \left[\frac{1}{(k_0 r)^2} + \frac{-j}{(k_0 r)^3} \right] e^{-jk_0 r} \quad (1)$$

$$E_\theta^i = \frac{\eta_0 k_0^2}{4\pi} I_e l \cdot \sin\theta \left[\frac{j}{k_0 r} + \frac{1}{(k_0 r)^2} + \frac{-j}{(k_0 r)^3} \right] e^{-jk_0 r} \quad (2)$$

$$H_\phi^i = \frac{k_0^2}{4\pi} I_e l \cdot \sin\theta \left[\frac{j}{k_0 r} + \frac{1}{(k_0 r)^2} \right] e^{-jk_0 r} \quad (3)$$

The time-averaged force exerted by such a field on a Rayleigh particle with polarizability $\alpha_{ee} = \alpha'_{ee} - j\alpha''_{ee}$, is given by [16]

$$\mathbf{F} = \frac{\alpha'_{ee}}{4} \nabla \left| \mathbf{E}^i \right|^2 + \alpha''_{ee} \left\{ \eta_0 k_0 \mathbf{S}^i + \frac{\omega}{2\varepsilon_0} \nabla \times \mathbf{L}_S^i \right\} \quad (4)$$

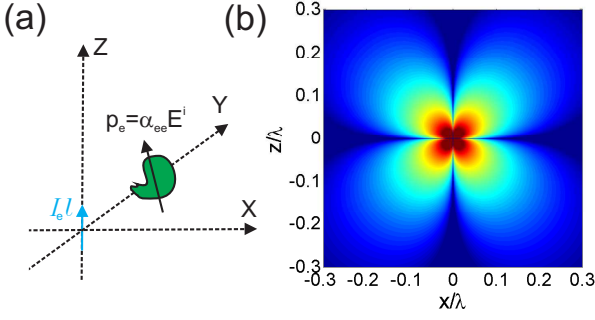The first addend constitutes the gradient force that at-

FIG. 1. (Color online) (a) Sketch of a Hertzian dipole illuminating a dipolar particle. (b) Color map of the magnitude of the spin angular momentum density: $\mathbf{L}_S^i$, in the xz-plane (arbitrary units, blue to red scale). The symbols $\otimes$ and $\odot$ represents the ingoing and outgoing directions, respectively, of $\mathbf{L}_S^i$ at each quadrant.

tracts (repels) particles with $\alpha'_{ee} > 0$ ($\alpha'_{ee} < 0$) from the regions of maximal electric field intensity, and thus enables the trapping of non-resonant particles ($\alpha'_{ee} \gg \alpha''_{ee}$) at the source region. In contrast, the second addend is usually called the absorption-scattering force. It is proportional to α''_{ee}, which, in turn, is proportional to the particle extinction cross-section. The absorption-scattering force is itself divided into two components: The first one constitutes the radiation pressure; it is proportional to the time-averaged Poynting vector of the exciting field, $\mathbf{S}^i = \frac{1}{2}\mathrm{Re}\left[\mathbf{E}^i \times \left(\mathbf{H}^i\right)^*\right]$. Therefore, it is a FF force component that pushes passive particles ($\alpha''_{ee} > 0$) radially away from the source; and it is angularly weighted by the radiation power pattern of the dipole: $\sin^2\theta$. The second component is the curl-spin force, which is a non-conservative force field associated with a non-uniform distribution of the angular momentum of the electromagnetic field [16]. Since this component is usually disregarded (e.g., see Ref. 19), it will be discussed here into more detail.

The term $\mathbf{L}_S^i = \frac{\varepsilon_0}{2j\omega}\left(\mathbf{E}^i\right)^* \times \mathbf{E}^i$ represents the spin component of the angular momentum density, which is the component associated to rotation of the polarization and is the only one that can be measured through Stoke's parameters [20, 21]. We have found that for Hertzian dipole fields it can be written as

$$\mathbf{L}_S^i = \frac{2\varepsilon_0}{\omega}\left|\frac{\eta_0 k_0^2}{4\pi}I_e l\right|^2 \frac{\sin\theta\cos\theta}{(k_0 r)^3}\,\widehat{\phi} \qquad (5)$$

Due to the symmetry of the dipole field components, Eqs. (1)-(3), a net $\mathbf{L}_S^i$ results only from the phase-shift between the term $(k_0 r)^{-1}$ from the polar angle component and the term $(k_0 r)^{-2}$ from the radial component. Consequently, the curl-spin force produced by a Hertzian dipole has only a NF impact. Moreover, the $\sin\theta\cos\theta$ factor ensures that $\mathbf{L}_S^i$ vanishes along the z-axis and in the xy-plane, where the field is linearly polarized. Finally,

$\mathbf{L}_S^i$ has only an azimuthal component and possesses perfect azimuthal symmetry. All of these properties are evidenced in Fig. 1(b), which depicts the magnitude and direction of $\mathbf{L}_S^i$ in the xz-plane.

The associated curl-spin force: $\mathbf{F}_{\mathrm{cs}} = \frac{\omega\alpha''_{ee}}{2\varepsilon_0}\nabla \times \mathbf{L}_S^i$, can be computed readily. Moreover, the directions along which the force is exerted can be intuitively understood by bearing in mind the description of $\mathbf{L}_S^i$ given by Fig. 1(b). Wherever $\mathbf{L}_S^i$ reverses its direction, the force components add and produce a net force. As schematically illustrated in Fig. 2(a), this produces a net force along the $\pm z$-axis, as well as an attractive force in the xy-plane. This behavior is verified in Figs. 2(b) and 2(c), which represent $\mathbf{F}_{\mathrm{cs}}$ as a function of the position of the particle centered on the xz- and xy-planes, respectively. Note that, due to the perfect azimuthal symmetry of the problem, the plot in the xz-plane already contains all the information of the 3D problem. Specifically, the color at each point defines the magnitude of the force produced if the particle were placed at such a position, while the arrows indicate the direction of this force. The force color maps have been normalized to 100 pN, a typical trapping force for optical tweezers [1], and are portrayed in a dB scale. The source was assumed to have the current moment $I_e l = 10^{-3}\lambda$ A. The particle was taken to be a dielectric sphere of $a = 0.025\lambda$ radius and relative permittivity $\varepsilon_s = 4$. It has the polarizability [17]:

$$\alpha_{ee} = j\frac{6\pi\varepsilon_0}{k_0^3}\left[-1 + j\frac{3}{2}\frac{1}{(k_0 a)^3}\frac{\varepsilon_s + 2}{\varepsilon_s - 1}\right]^{-1} \qquad (6)$$

Figs. 2(a)-(c) reveal that $\mathbf{F}_{\mathrm{cs}}$ pushes the particle towards the xy-plane and then attracts it towards the source. Therefore, the curl-spin force produced by a localized source is an attractive component of the absorption scattering force that can be exploited in NF electromagnetic trapping.

III. NEAR-FIELD TRAPPING THROUGH CURL-SPIN FORCES

The total force exerted on the particle is given by the superposition of the gradient, radiation pressure and curl-spin forces, i.e., Eq. (4). The balance between such force components is imposed by the relationship between the real, α'_{ee}, and imaginary, α''_{ee}, parts of the particle polarizability. For example, since $\alpha'_{ee} \gg \alpha''_{ee}$ for the aforementioned non-resonant particle, the gradient force is the dominant one. This is evidenced in Fig. 3(a) and 3(b), which represent, respectively, the total force acting on the particle centered on the xz- and xy-planes.

The situation changes radically for resonant particles. Consider, for example, a dielectric sphere whose relative permittivity is described by the Drude dispersion model: $\varepsilon_s = 1 - \omega_p^2/\left(\omega^2 - j\gamma_c\omega\right)$, where ω_p is the plasma frequency and γ_c is the collision frequency. Fig. 4 depicts α_{ee} as a function of the normalized frequency ω/ω_p for
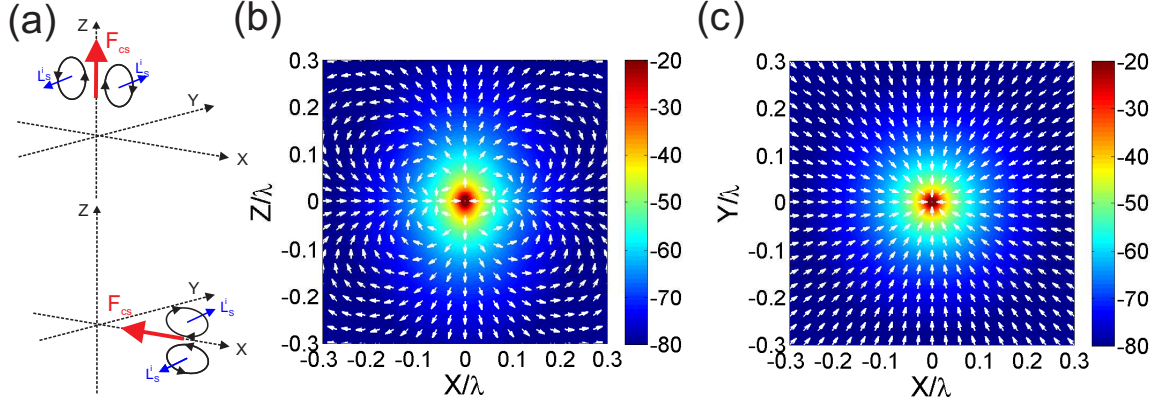
FIG. 2. (Color online) (a) Sketches of the curl-spin force $\mathbf{F}_{cs}$ originating from the spin angular momentum density: $\mathbf{L}_S^i$. Color maps and quiver plots (arrows) of $\mathbf{F}_{cs}$ produced by a Hertzian dipole with current moment $I_e l = 10^{-3} \lambda\,\mathrm{A}$ interacting with a dielectric sphere (radius $a = 0.025\lambda$ and relative dielectric constant $\varepsilon_s = 4$) that is centered on the (b) xz- and (c) xy-planes.
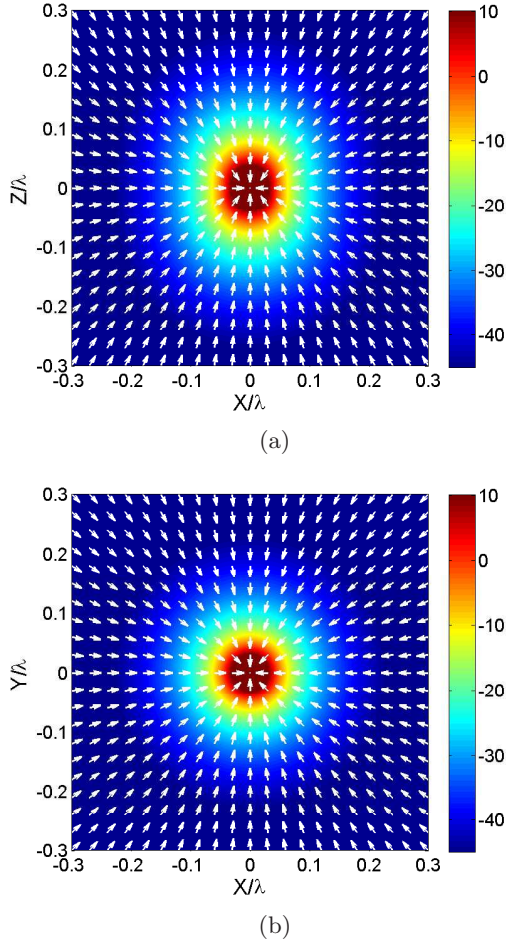

FIG. 3. (Color online) Color maps and quiver plots (arrows) of the total force exerted by a Hertzian dipole with current moment $I_e l = 10^{-3} \lambda\,\mathrm{A}$ on a $\varepsilon_s = 4$ dielectric sphere of radius $a = 0.025\lambda$ centered on the (a) xz- and (b) xy-planes.

$\gamma_c = \omega_p/200$. The resonant frequency, marked by the vertical dashed line, is found at $\omega/\omega_p \simeq 0.5775$. At this point, α_{ee}'' is maximized and α_{ee}' goes to zero. Consequently, the gradient force contribution vanishes. The total force exerted on the particle is depicted in Figs. 5(a) and 5(b). It is apparent that the magnitude of the force is enhanced in comparison to the non-resonant case. Moreover, the radiation pressure and curl-spin forces compete at resonance to repel the particle from or attract it to the source. Since the latter is dominant in the near field, there is a region of attractive forces near the source that enables NF trapping when a resonance occurs. Since the curl-spin force, which is the main attractive mechanism, is divergence-free, it could be questioned whether this force component alone can lead to stable trapping. However, as it will be demonstrated in Section IV, all of the particle escape routes converge into the source region of the trapping device in this NF scenario when both the curl-spin and radiation pressure forces are taken into account, enabling stable trapping. As this fact becomes more evident for finite-size sources, numerical and stability analyses of the NF trapping enabled by a finite-length dipole antenna are presented in Section IV.

Note that radiation pressure and curl-spin forces created by the Hertzian dipole fields perfectly cancel each other at a distance $k_0 r = \sqrt{2}$ from the dipole in the xy-plane. This means there is a ring in the xy-plane of zero force, which exists at a distance of approximately 0.23λ (see Fig. 5(b)). While this fixed ring distance has been derived for the Hertzian dipole source, more general zero-force curves could be designed and enhanced with more sophisticated and optimized localized source distributions.

Since the forces at a resonance are significantly larger than those associated with non-resonant cases, the attractive forces operating at the resonance could lead to more efficient and selective electromagnetic traps. Furthermore, because the particle-electromagnetic field interactions are enhanced at a resonance, they can be com-
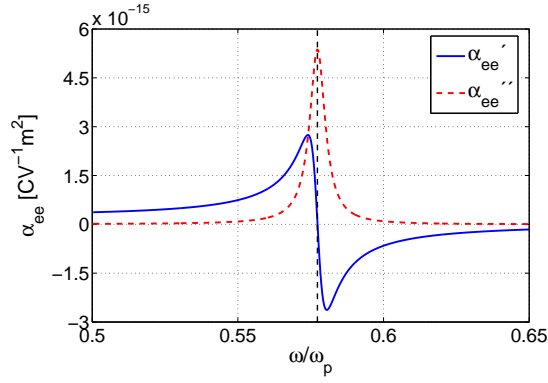
FIG. 4. Polarizability, α_{ee}, of a Drude dispersive dielectric sphere with collision frequency $\gamma_c = \omega_p/200$ as a function of the normalized frequency ω/ω_p .
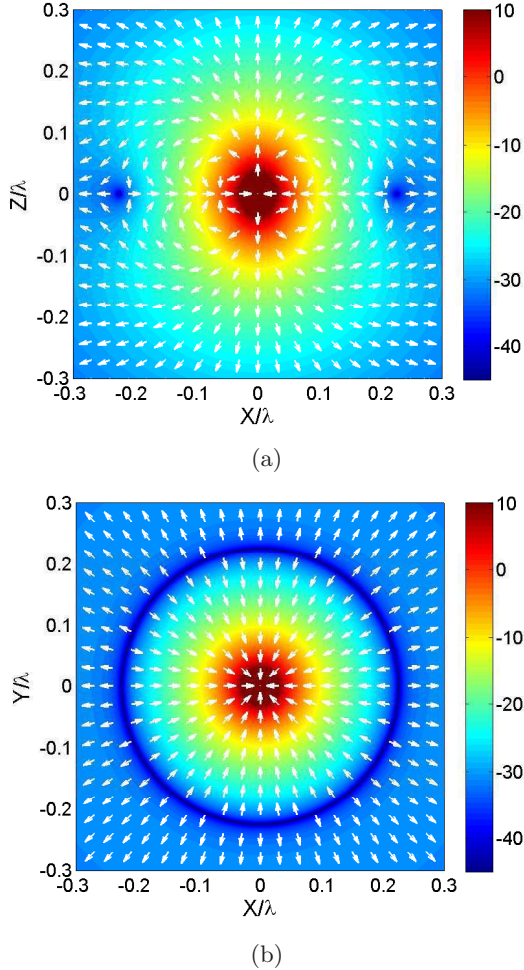

(a)

(b)

FIG. 5. (Color online) Color maps and quiver plots (arrows) of the total force exerted by a Hertzian dipole with current moment $I_e l = 10^{-3}\lambda\,$A on a Drude dispersive dielectric sphere of radius $a = 0.025\lambda$ with collision frequency $\gamma_c = \omega_p/200$ centered on the (a) xz- and (b) xy-planes.

bined with the creation of the attractive forces for a wide range of applications. For example, Fig. 6 is a color map of the power absorbed by the dispersive dielectric particle when its center is positioned on the x-axis, as a function of the normalized frequency ω/ω_p and the separation distance: X/λ. The absorbed power was normalized to the power radiated by the dipole source in free-space $P_0 = \eta_0/\left(12\pi\right)\left|I_e k_0 l\right|^2$ and portrayed on a dB scale. Fig. 6 ratifies that the absorbed power is maximized at the resonance. Note that the solid black line superimposed on the power color map corresponds to the frequency-position pairs where the total force is zero. For example, this solid black line cuts the resonance dashed line at the value $X/\lambda = 0.23$, corresponding to the zero-force ring in Fig. 5(b). In general, the particle is subjected to attractive (repulsive) forces when it is placed at a frequency-position point to the left (right) of the solid black line. Since attractive forces are present at the frequency at which the absorbed power is maximized, any system of energy exchange can be optimized to achieve the situation where the particle tends to be attracted to the source at the same time that the power flows maximally from the source to the particle.

Moreover, it has been found that, since the scattered power is maximized at a particle resonance, resonant particles (e.g., spherical core-shell structures) enhance the radiation from localized sources (e.g., Hertzian dipoles)[22, 23]. In this manner, it can be concluded that the attractive behavior of the curl-spin force can be tailored to cause the source and coupled resonator pair to be stably stuck together. This result suggests that the attractive behavior of the curl-spin force can coexist with enhancements in the radiation from the sources. These enhancements are often discussed in association with the Purcell effect[24]; this connection is left to future studies. Additionally, the source and resonant particle combination could be co-designed to achieve more effective and selective traps, e.g., self-induced trapping mechanisms[25]. Note that a resonant dielectric particle was selected for this discussion solely for mathematical convenience. In fact, any resonant particle exhibits a similar resonant polarizability, and the results revealed here can be extrapolated to a large number of structures.

Regions where the net force is zero can also be of interest for a number of applications. Let us follow the dark-solid line in Fig. 6. Below the resonance, attractive NF gradient and curl-spin forces compete against the repulsive FF radiation pressure. This balance of forces creates a zero-force ring in the xy-plane, corresponding to the transition of the total force from attractive to repulsive. Such a ring is maintained even at the resonance due to curl-spin forces. Interestingly, the repulsive gradient forces above the resonance create a bend in the dark-solid line in Fig. 6. In this manner, there is a frequency range in which two zero-force rings are created. To emphasize this fact, Fig. 7 represents the total force exerted on a particle at the normalized frequency $\omega/\omega_p = 0.5778$. The two zero-force rings on the xy-plane correspond to tran-
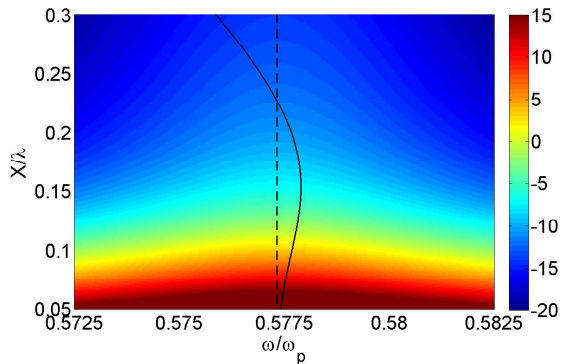
FIG. 6. (Color online) Color map of the power absorbed by the dispersive sphere, when it is centered on the x-axis, as a function of the distance of separation: X/λ, and normalized frequency ω/ω_p. The dark-solid line indicates the position-frequency pairs where the total force is zero.

sitions between the dominant regions of repulsive gradient → attractive curl-spin → repulsive radiation pressure forces. The force vectors indicate that the inner ring is stable (in the sense that all neighbouring forces point towards the ring). Thus, particles can be stably trapped inside the ring, i.e., the particles are trapped in the vicinity of (but not exactly in) the source, protecting the trapping device from any damage that could be produced manipulating the trapped particles. Moreover, once the particle is trapped within the ring, any external action could force the particle to move near the source and remain within the ring, extending the scope of the experiments to study the characteristics of moving and rotating particles.

IV. STABILITY ANALYSIS

Since the curl-spin force arises from the curl of the spin angular momentum density, Eq. (4), it can be concluded that the curl-spin force field is divergence-free and, consequently, the streamlines of this force vector field are described by closed loops. Therefore, the integration of the flux of such a vector field through a surface enclosing a finite volume is zero, and any direction in which a force vector points towards the interior of this finite volume must be compensated by a force vector pointing out of the volume in the opposite direction. In particular, this means that there are escape routes for the particles initially trapped within the volume. As the optical Earnshaw's theorem [26] would then suggest, no stable optical trapping is possible by means of curl-spin forces alone.

However, this non-stable behavior can be overcome in a near-field scenario when all of the escape routes converge into the source region of the trapping device. Then, if the actual source region is inaccessible to the trapped particles because their physical sizes are too large or because the trapping device might be covered by a protective
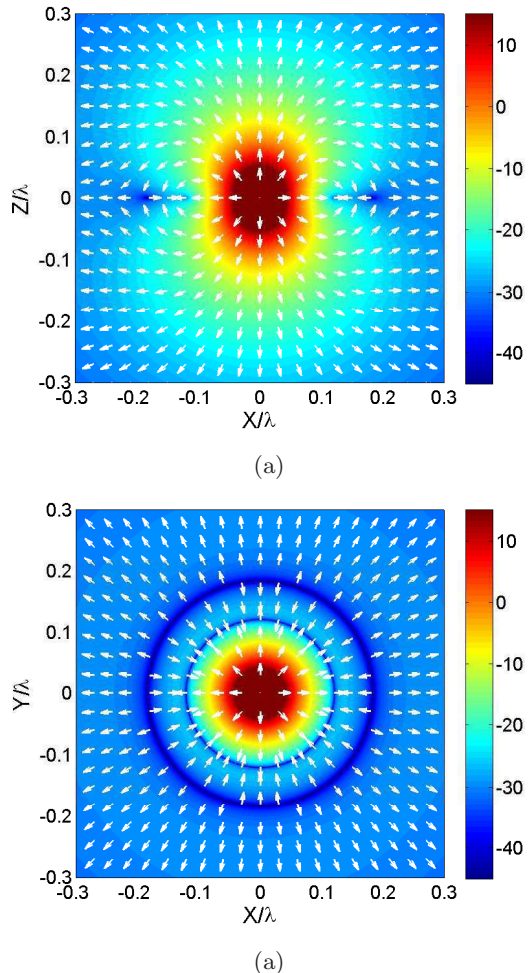

(a)

(a)

FIG. 7. (Color online) Color map and quiver plot (arrows) of the forces exerted by a Hertzian dipole with current moment $I_e l = 10^{-3}\lambda$ A on the dispersive dielectric sphere of radius $a = 0.025\lambda$ centered on the (a) xz- and (b) xy-planes. Drude model with collision frequency $\gamma_c = \omega_p/200$ evaluated at $\omega/\omega_p = 0.5778$.

layer, the resulting mechanical forces prevent the particles from escaping the near-field region. Thus, in contrast to the more standard far-field scenario [26], the near-field (divergence-free) curl-spin forces, in conjunction with the gradient and radiation pressure force fields (which are *not* divergence-free), can be engineered in practice to enable stable trapping.

A. Numerical Stability Analysis

Let us examine another canonical example to illustrate this point further. Specifically, consider a finite-size electric dipole antenna oriented along the z-axis and excited with a sinusoidal current distribution centered at the ori-

gin of the coordinates:

$$I\left(z\right) = I\left(0\right)\frac{\sin\left(k_0 L - k_0 |z|\right)}{\sin\left(k_0 L\right)} \tag{7}$$

This is the dominant current distribution function for a thin-wire antenna [18]. The current extends over the entire length: $2L$, and $I\left(0\right)$ is the current distribution at the center of the dipole (origin of the coordinates). It is assumed to be set to $1\,\mathrm{mA}$.

Fig. 8 depicts the curl-spin force produced by a sinusoidal current distribution with $L = \lambda/10$ as a function of the particle position centered on the xz-plane. Note that due to the perfect azimuthal symmetry of the fields, such a figure represents a complete description of the whole 3D problem. It is clear from Fig. 8 that the curl-spin force pushes the particle towards the xy-plane, and then attracts it towards the actual driving point of the antenna. Fig. 8 also confirms that the curl-spin force field is divergence-free since its streamlines would form closed loops.

However, it is also evident that the only escape routes for a particle are those directed along the z-axis. Consequently, any escaping particle would have to circulate within the source region to eventually depart from the trap. This is in general not possible due to the physical size of the trapping device, i.e., the dipole antenna.

Let us assume, for example, that the trapping device volume is confined to be within the solid black contour depicted in Fig. 8. In this manner, as a particle is accelerated towards the source region of the dipole, it will collide against its surface at a given time t_c. Assuming that the trapping device is initially at rest, the velocities perpendicular to its surface and to that of the particle after the collision, respectively, $\mathbf{v}_\perp^p\left(t_c^+\right)$ and $\mathbf{v}_\perp^s\left(t_c^+\right)$, are functions of the trapping device and particle masses: m_p and m_s, as well as the velocity of the particle before the collision: $\mathbf{v}_\perp^p\left(t_c^-\right)$. They can be written as [27]

$$\mathbf{v}_\perp^p\left(t_c^+\right) = \mathbf{v}_\perp^p\left(t_c^-\right)\frac{m_p - C_R m_s}{m_p + m_s} \tag{8}$$

$$\mathbf{v}_\perp^s\left(t_c^+\right) = \mathbf{v}_\perp^p\left(t_c^-\right)\frac{m_p\left(1 + C_R\right)}{m_p + m_s} \tag{9}$$

where C_R is the coefficient of restitution, being $C_R = 1$ for a perfect elastic collision and $C_R = 0$ for a perfect inelastic collision. In general, a particle might rebound off the dipole and return back to it several times before losing its kinetic energy and becoming stuck to the antenna. However, such an effect is actually negligible for small initial particle speeds, i.e., $\mathbf{v}_\perp^p\left(t_c^+\right), \mathbf{v}_\perp^s\left(t_c^+\right) \approx 0$ for small $\mathbf{v}_\perp^p\left(t_c^-\right)$ and $m_p \ll m_s$. Therefore, it can be assumed that once a particle comes in contact with the surface of the trapping device, it stops its motion perpendicular to it, i.e., once the particle encounters the surface of the trapping device, the electromagnetic force, which was directing the particle to it along its normal, will be
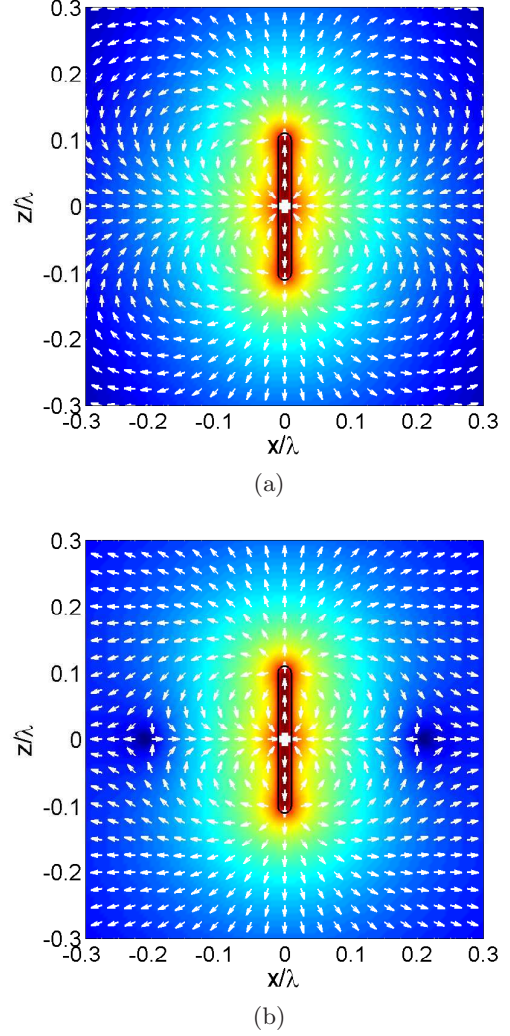

(a)

(b)

FIG. 8. (Color online) Colormap and quiver plot (arrows) of (a) the curl-spin $\mathbf{F}_{\mathrm{cs}}$ and (b) $\mathbf{F}_{\mathrm{cs}} + \mathbf{F}_{\mathrm{rp}}$ force fields in the xz-plane (arbitrary units, blue to red scale) produced by an antenna with $L = \lambda/10$ and driven with a sinusoidal current distribution.

compensated by the corresponding mechanical reaction force acting perpendicular to and away from the dipole's surface. As for the forces parallel to the trapping device surface, it can be inferred from the directions of the curl-spin force depicted in Fig. 8(a) that they push the particle towards the dipole excitation region, an equilibrium position in the xy-plane.

Therefore, it can be concluded that any particle located on the surface of the trapping device in the xy-plane is stably trapped there. In other words, any displacement of the particle from such an equilibrium position results in a restoring force that pushes the particle back to it. Furthermore, if the curl-spin force were acting on its own, any particle in the vicinity of the dipole would end up stably trapped on it in the xy-plane independent of its initial location. Moreover, any ambient damping

of the particle motion would enhance the stability of this trapping behavior.

Despite this force field action, the additional presence of the radiation pressure force actually limits the extent to which the particles can be trapped. Note that, unlike the curl-spin force, the radiation pressure force is not divergence-free. In fact, since it follows the flow of radiated power, the radiation pressure force field emanates from the sources and pushes passive particles away from them. The superposition of the curl-spin and radiation pressure forces results in the total absorption scattering force, $\mathbf{F}_{as} = \mathbf{F}_{cs} + \mathbf{F}_{rp}$. Fig. 8(b) depicts this absorption scattering force as a function of the particle position in the xz-plane. It can be concluded by observation that, unlike the curl-spin force, the streamlines of the absorption scattering vector field do not form closed loops and there are force lines that simply propagate away from the sources.

Consequently, a particle acted on by $\mathbf{F}_{as}$ will either reach the source and be trapped by its combination with the mechanical forces produced by the dipole antenna or it will simply be pushed away from the dipole as a function of its initial position. To give a more complete picture of the trapping performance, Fig. 9 represents the region of initial points whose trajectories converge to the equilibrium point (red color), i.e., the collection of initial points that lead to a stable trapping at the surface of the source of the field in the xy-plane. The volume occupied by the trapping device has been colored grey, the magnitude of the absorption scattering force is given in color, and its vector field are also depicted.

To generate this plot, the particle trajectories were numerically calculated by means of the Verlet algorithm [28]

$$\mathbf{r}\left(t+\triangle t\right) = 2\mathbf{r}\left(t\right) - \mathbf{r}\left(t-\triangle t\right) + \triangle t^2 \frac{\mathbf{F}_{as}\left(t\right)}{m_p} + \mathcal{O}\left(\triangle t^4\right)$$
(10)

where the time has been discretized with time step $\triangle t$, and the initial state is specified as $\mathbf{r}_0 = \mathbf{r}\left(t=0\right) = \mathbf{r}\left(t=-\triangle t\right)$. The trajectories have been computed with the particle mass: $m_p = 1\,\mu\text{g}$ and the time step: $\triangle t = 1\,\mu\text{s}$. Note that the driving force is independent of the initial velocity for non-relativistic speeds and in the absence of any ambient damping, $\mathbf{F}_{as}\left(t\right) = \mathbf{F}_{as}\left(\mathbf{r}\left(t\right)\right)$. Thus, the force exerted on the particle as a function of its initial position corresponds to the colormap depicted in Fig. 8(b).

Fig. 9 demonstrates that, aside from the volume of the trapping device, there is a simply connected set of initial points whose trajectories converge to the source region, which reassures the concept of stable trapping facilitated through the curl-spin forces. To further illustrate this fact, Figs. 9(b) and 9(c) depict a sample of trajectories (represented as solid black lines) for several different initial points (represented as red X markers). In addition, the trajectories have been superimposed on the force field plot to help understand the correlation between the force exerted on the particle and its trajectory. The outer boundary of the trapping region, i.e., the set of initial points whose trajectories converge to the source region, has been depicted with a closed red curve.

Fig. 9(b) corresponds to trajectories of particles that become trapped. Since the particles are stably trapped at the xy-plane, any particle initially located on the x-axis has a trajectory that is a straight line towards the source region. In contrast, if the initial point is not on the xy-plane, the particles feel a trapping force that points towards the xy-plane and, hence, approach the source region in an oscillatory manner. On the other hand, Fig. 9(c) illustrates the trajectories of particles that are pushed away from the source region. In general, a trajectory will never converge towards the source region if its initial position is far enough away from it so that the radiation pressure force dominates the total force $\mathbf{F}_{as}$. Naturally, the trapping region would be expanded somewhat by the presence of ambient damping since it would reduce the inertia produced by the initial repulsive force.

B. Analytical Stability Analysis

The linear stability analysis presented in Ref. 29 is used here to further assess the stability of the proposed NF trapping configuration. Let us hypothesize that the particle is trapped against the surface of the trapping device and is located at the position $\mathbf{r}_0 = x_0\widehat{\mathbf{x}}$. If there is a displacement $\triangle\mathbf{r}$ from the position $\mathbf{r}_0$, the equation of motion of the particle can be written as

$$m_p\partial_t^2\triangle\mathbf{r} + \gamma\partial_t\triangle\mathbf{r} = \mathbf{F}_{em} + \mathbf{F}_{mech}$$
(11)

where γ is the damping constant for the particle in the suspending medium, $\mathbf{F}_{em}$ is the electromagnetic force, and $\mathbf{F}_{mech}$ represents the mechanical force acting on the particle due to its collision with the surface of the trapping device. For non-relativistic speeds, the electromagnetic force is a mere function of the particle position $\mathbf{F}_{em} = \mathbf{F}_{em}\left(\triangle\mathbf{r}\right)$. However, due to the non-linear dependence of such a force with the particle's position, (11) is in general a non-linear equation without any known analytical solution. Despite this, the equation of motion can be linearized for small $\triangle\mathbf{r}$ by taking a Taylor series expansion of $\mathbf{F}_{em}$ at the equilibrium point and keeping only the two first terms:

$$m_p\partial_t^2\triangle\mathbf{r} + \gamma\partial_t\triangle\mathbf{r} \approx \mathbf{F}_{em}\left(\mathbf{r}_0\right) + \left(\triangle\mathbf{r}\cdot\nabla\right)\mathbf{F}_{em} + \mathbf{F}_{mech}$$
(12)

If the particle is resonant and its position is close to the source, the $\left(k_0 r\right)^{-4}$ term of the absorption-scattering force is dominant. In particular, in the NF of a Hertzian dipole source, $\mathbf{F}_{em}$ can be written in closed form as

$$\mathbf{F}_{em} \approx A\frac{\left(2\text{cos}^2\theta - \text{sin}^2\theta\right)\widehat{\mathbf{r}} + 2\text{sin}\theta\text{cos}\theta\,\widehat{\boldsymbol{\theta}}}{r^4}$$
(13)

where $A = \alpha_{ee}''\left|\eta_0 I_e l/\left(4\pi\right)\right|^2$ is a real constant with units: $\text{N}\cdot\text{m}^4$, that takes on positive values for passive particles.
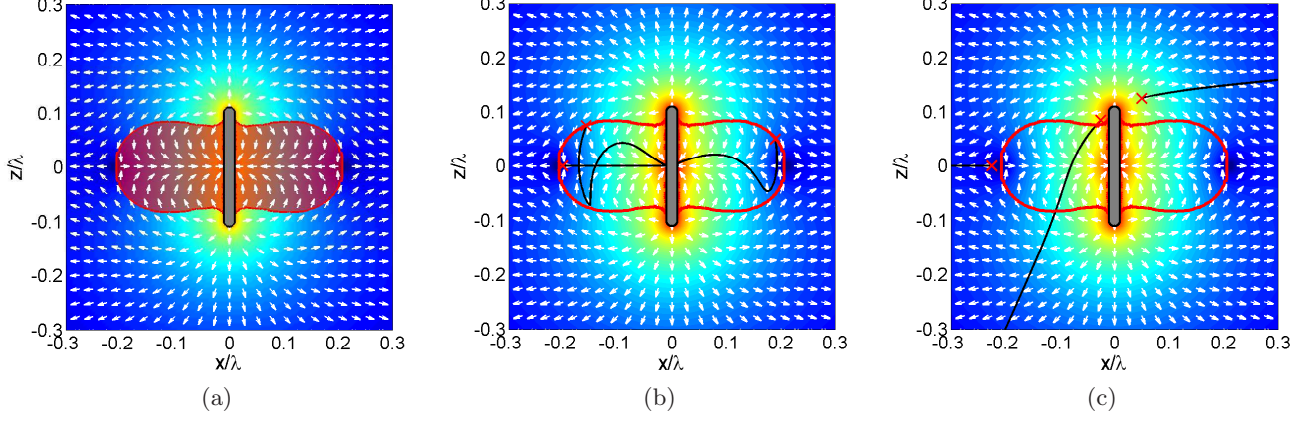
FIG. 9. (Color online) (a) Region containing the initial points whose trajectories yield stable trapping (red color). The region is superposed to the colormap and quiver plot (arrows) of $\mathbf{F}_{\mathrm{as}}$ in the xz-plane (arbitrary units, blue to red scale) produced by an antenna with $L = \lambda/10$ and driven with a sinusoidal current distribution. (b) & (c) Collection of particle trajectories (solid black lines) as a function of their initial points (red X markers) for (b) convergent and (c) divergent trajectories.

According to (13), the forces at $\mathbf{r}_0$ can be expressed in Cartesian coordinates as follows

$$F_z^{\mathrm{em}}(\mathbf{r}_0) = 0 \tag{14}$$

$$F_x^{\mathrm{em}}(\mathbf{r}_0) = -\frac{A}{|x_0|^4} \tag{15}$$

On the one hand, the zero value of the z-component of the force ensures that the particle is at an equilibrium position with respect to the z-th coordinate. On the other hand, the negative value of the x-th force confirms that the electromagnetic force pushes the particle against the surface of the trapping device.

Taking the partial derivatives of $F_z^{\mathrm{em}}(\mathbf{r}_0)$ and $F_x^{\mathrm{em}}(\mathbf{r}_0)$ given by (13) and particularizing the expressions to the trapping point, one has

$$\partial_x \{F_z^{\mathrm{em}}(\mathbf{r}_0)\} = \partial_z \{F_x^{\mathrm{em}}(\mathbf{r}_0)\} = 0 \tag{16}$$

$$\partial_z \{F_z^{\mathrm{em}}(\mathbf{r}_0)\} = -\frac{2A}{|x_0|^5} \tag{17}$$

$$\partial_x \{F_x^{\mathrm{em}}(\mathbf{r}_0)\} = \frac{4A}{|x_0|^5} \tag{18}$$

Since all of the cross partial derivatives are zero, the equation of motion is decoupled into two independent equations for the $\triangle z$ and $\triangle x$ displacements. In addition, the negative value of $\partial_z \{F_z^{\mathrm{em}}(\mathbf{r}_0)\}$ demonstrates that the particle is at a stable equilibrium position with respect to the $\triangle z$ displacements. Specifically, the equation of motion corresponding to $\triangle z$ displacements reduces to

$$m_p \partial_t^2 \triangle z + \gamma \partial_t \triangle z + \frac{2A}{|x_0|^5} \triangle z = 0 \tag{19}$$

which corresponds to the equation of motion of a position-dependent damped harmonic oscillator. Since $2A/|x_0|^5 > 0$, the electromagnetic force acts as a restoring force that confines the particle to the xy-plane. Therefore, the trap is stable with respect to the $\triangle z$ displacements. Furthermore, the restoring force becomes larger as the trapping point is closer to the actual source region. In fact, the restoring behavior would only break down at the exact limit $x_0 = 0$, ratifying our conclusion that the only escaping route from xy-plane is to circulate across the actual source region.

Secondly, the equation of motion for the $\triangle x$ displacements can be written as

$$m_p \partial_t^2 \triangle x + \gamma \partial_t \triangle x + \frac{A}{|x_0|^4}\left(1 - \frac{4\triangle x}{|x_0|}\right) = F_x^{\mathrm{mech}} \tag{20}$$

Note that the non-linear electromagnetic force is always negative. This means the condition: $|\triangle x| < |x_0|/4$, must be imposed to avoid a non-physical inversion of the force sign produced by the linearization. Due to the presence of F_x^{mech}, the solution to this equation of motion is a piecewise function. Specifically, the particle starts at a given displacement $\triangle x_0$ with zero velocity, $v_p(t=0) = 0$. Then, the electromagnetic force accelerates the particle towards the trapping device until it collides against its surface with velocity $v_p(t=t_c^-)$. Next, the particle will rebound off the trapping device with velocity $v_p(t=t_c^+)$, and it propagates against the electromagnetic force until it reaches again zero velocity at a given displacement $\triangle x_1$. If $\triangle x_1 < \triangle x_0$, this cycle is repeated with increasingly smaller displacements and the trap is stable.

It can be demonstrated that this is the case even in the absence of ambient damping. To this end, let us neglect ambient damping and consider a spatially non-uniform acceleration $a(\triangle x) = -\frac{A}{m_p|x_0|^4}\left(1 - \frac{4\triangle x}{|x_0|}\right)$. First, since

$a = \partial_t v$, the velocity of the particle in the instant before the collision can be found by integration:

$$\int_0^{v_p(t_c^-)} v\,dv = -\frac{A}{m_p |x_0|^4} \int_{\Delta x_0}^0 \left(1 - \frac{\triangle x}{|x_0|}\right) d\triangle x \quad (21)$$

Next, the velocity of the particle after the collision can be evaluated as in (8). For $m_p \ll m_s$ it can be simply written as $v_p\left(t_c^+\right) = -C_R v_p\left(t_c^-\right)$. Finally, following a process that is the inverse to (21), the new point at which the velocity is zero, Δx_1 can be found from

$$\int_{v_p(t_c^+)}^0 v\,dv = -\frac{A}{m_p |x_0|^4} \int_0^{\Delta x_1} \left(1 - \frac{\triangle x}{|x_0|}\right) d\triangle x \quad (22)$$

In this manner, the relationship between the initial displacement Δx_0 and the new point of zero velocity, Δx_1, is found to be

$$\Delta x_0 - \frac{\Delta x_0^2}{|x_0|} = C_R^2 \left(\Delta x_1 - \frac{\Delta x_1^2}{|x_0|}\right) \quad (23)$$

This equality is sufficient to prove that $\Delta x_1 \leq \Delta x_0$. To this end, let us define the function $f\left(\Delta x\right) = \Delta x - \frac{\Delta x^2}{|x_0|}$. Since $C_R \leq 1$, it can be concluded that $f\left(\Delta x_1\right) \leq f\left(\Delta x_0\right)$. It was pointed out that only displacements satisfying $|\Delta x| < |x_0|/4$ lead to physical solutions. Consequently, it can be concluded that $f\left(\Delta x\right)$ grows along with Δx, i.e., $\partial_{\Delta x}\left\{f\left(\Delta x\right)\right\} = 1 - 2\Delta x/|x_0| > 0$. Therefore, $f\left(\Delta x_1\right) \leq f\left(\Delta x_0\right)$ is sufficient to demonstrate that $\Delta x_1 \leq \Delta x_0$, which proves that the trap is also stable with respect to Δx displacements.

V. CONCLUSIONS

To summarize, this paper has introduced the concept of electromagnetic trapping enabled by the near-field curl-spin forces produced by a localized source. It was illustrated how more effective and selective electromagnetic traps could be created using this particle-resonance force effect and how it could lead to benefits in other applications, such as boosting the energy transfer between and bringing stability to coupled resonant radiators. It also was demonstrated that the balance between the different force components results in the formation of zero-force rings and stable NF force zones around the sources, which suggests new and dynamic forms of electromagnetic trapping. Moreover, the stability of the electromagnetic trap was numerically and analytically assessed.

[1] J. Nilsson, M. Evander, B. Hammarström, and T. Laurell, Anal. Chim. Acta **649**, 141 (2009).
[2] J. P. Desai, A. Pillarisetti, and A. D. Brooks, Annu. Rev. Biomed. Eng. **9**, 35 (2007).
[3] J. R. Moffitt, Y. R. Chemla, S. B. Smith, and C. Bustamante, Annu. Rev. Biochem. **77**, 205 (2008).
[4] M. Dienerowitz, M. Mazilu, and K. Dholakia, J. Nanophoton. **2**, 1875 (2008).
[5] T. L. Gustavson, A. P. Chikkatur, A. E. Leanhardt, A. Görlitz, S. Gupta, D. E. Pritchard, and W. Ketterle, Phys. Rev. Lett. **88**, 020401 (2001).
[6] A. Ashkin, Phys. Rev. Lett. **24**, 156 (1970).
[7] D. G. Grier, Nature **424**, 810 (2003).
[8] A. Ashkin, IEEE J. Sel. Topics Quantum Electron. **6**, 841 (2000).
[9] D. Ruffner and D. Grier, Phys. Rev. Lett. **109**, 3903 (2012).
[10] A. Novitsky, C.-W. Qiu, and H. Wang, Phys. Rev. Lett. **107**, 3601 (2011).
[11] A. Novitsky, C.-W. Qiu, and A. Lavrinenko, Phys. Rev. Lett. **109**, 3902 (2012).
[12] L. Novotny, R. X. Bian, and X. S. Xie, Phys. Rev. Lett. **79**, 645 (1997).
[13] M. Righini, P. Ghenuche, S. Cherukulappurath, V. Myroshnychenko, F. J. García de Abajo, and R. Quidant, Nano Lett. **9**, 3387 (2009).
[14] W. Zhang and O. J. F. Martin, in *Proceedings of the SPIE*, Vol. 7757 (2010) pp. 775712–7.
[15] A. Lovera and O. J. F. Martin, in *Proceedings of the SPIE*, Vol. 8097 (2011) pp. 80971Q–6Q.
[16] S. Albaladejo, M. Marqués, M. Laroche, and J. J. Sáenz, Phys. Rev. Lett. **102**, 3602 (2009).
[17] J. R. Arias-González and M. Nieto-Vesperinas, J. Opt. Soc. Am. A **20**, 1201 (2003).
[18] R. F. Harrington, *Time-Harmonic Electromagnetic Fields* (New York: McGraw-Hill, 1961).
[19] L. Novotny and B. Hecht, *Principles of Nano-Optics* (Cambridge Univ. Press, Cambridge, UK, 2006).
[20] J. H. Crichton and P. L. Marston, Elect. J. Differential Equations **04**, 37 (2000).
[21] P. L. Marston and J. H. Crichton, Phys. Rev. A **30**, 2508 (1984).
[22] S. Arslanagic, R. W. Ziolkowski, and O. Breinbjerg, Radio Science **42**, RS6S16 (2007).
[23] S. Arslanagić and R. W. Ziolkowski, Journal of Optics **12**, 024014 (2010).
[24] E. M. Purcell, Phys. Rev. **69**, 681 (1946).
[25] M. Barth and O. Benson, Appl. Phys. Lett. **89**, 253114 (2006).
[26] A. Ashkin and J. P. Gordon, Opt. Lett. **9**, 454 (1984).
[27] L. D. Landau and E. M. Lifshitz, *Mechanics, 3rd. ed.* (Pergamon Press, 1976).
[28] L. Verlet, Phys. Rev. **159**, 98 (1967).

[29] J. Ng, Z. Lin, and C. T. Chan, Phys. Rev. Lett. **104**, 103601 (2010).